ACS Catalysis

Research Article

pubs.acs.org/acscatalysis

Cr^{3+}−$Co_{0.054}Ni_{0.018}Mg_{0.93}O$ Solid-Solution Catalysts for High-Pressure Syngas Production: Effect of Chromium on the Reduction and Catalysis

Katsutoshi Nagaoka,*[,†,‡,§] Yosuke Abe,[†] Yusaku Hashimoto,[†] Takahiro Ishikawa,[†] Katsutoshi Sato,[†,⊥] Yusaku Takita,[†] Toshiya Wakatsuki,[∥] Masahiro Kunisu,[¶] Eri Suda,[¶] and Shin Inamoto[¶]

[†]Department of Applied Chemistry, Faculty of Engineering, Oita University, 700 Dannoharu, Oita 870-1154, Japan

[‡]JST CREST, Sanbancho 5, Chiyoda-ku, Tokyo 102-0075, Japan

[§]Elements Strategy Initiative for Catalysts and Batteries (ESICB), Kyoto University, Katsura, Kyoto 615-8520, Japan

[⊥]Energy Technology Research Institute, National Institute of Advanced Industrial Science and Technology (AIST), 1-1-1 Umezono, Tsukuba, Ibaraki 305-8568, Japan

[∥]JAPEX Research Center, Japan Petroleum Exploration Co., Ltd., 1-2-1 Hamada, Mihama-ku, Chiba 261-0025, Japan

[¶]Toray Research Center, Inc., 3-7 Sonoyama 3-chome, Otsu, Shiga 520-8567, Japan

Supporting Information

ABSTRACT: Adding Cr to heat-tolerant $Co_{0.054}Ni_{0.018}Mg_{0.93}O$ solid-solution catalysts for $CH_4/CO_2/H_2O$ reforming at 2.1 MPa allowed us to control the key properties determining the behavior of the supported catalysts, such as the reduction degree of the metal, metal particle size, and amount of exposed zerovalent metals. A small load of Cr [Cr/(Co + Ni) = 0.11 mol %] efficiently catalyzed Co^{2+} and Ni^{2+} reduction. This catalyst, which had abundant small alloy particles on the support material, resisted coking and oxidative deactivation, even under accelerated deterioration conditions. X-ray photoelectron spectroscopy, X-ray absorption near-edge structure, extended X-ray absorption fine structure, and scanning transmission electron microscopy−energy-dispersive X-ray measurements indicated that Cr existed as a trivalent cation in a $Cr_xCo_{0.054}Ni_{0.018}Mg_{0.93}O_{1+1.5x}$ solid solution, leading to the formation of a divalent cation vacancy and that Cr^{3+} was abundant on the surface of the catalyst particles after calcination at 1373 K. The Cr^{3+} destabilized Co^{2+} and Ni^{2+} in the solid solution, especially on the surface of the catalyst particles and, thus, promoted Co^{2+} and Ni^{2+} reduction. However, excess Cr^{3+} induced sintering of the catalyst particles, resulting in aggregation of alloy particles and, thus, in an increased risk of coking.

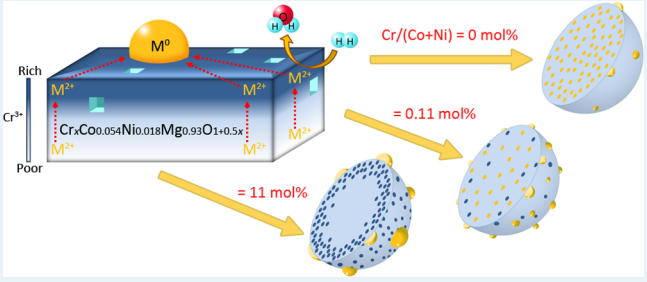

KEYWORDS: *tailoring catalyst, solid-solution, chromium, methane, reforming, syngas production*

INTRODUCTION

As petroleum resources continue to be depleted, the use of natural gas (CH_4) to produce chemicals and generate power will become increasingly necessary.[1] Reforming CH_4 with CO_2 ($CH_4 + CO_2 \rightleftarrows 2H_2 + 2CO$) or H_2O ($CH_4 + H_2O \rightleftarrows 3H_2 + CO$) to produce syngas ($CO + H_2$) is attracting renewed attention because advances in shale gas technology have increased the global supply of recoverable CH_4[2−6] and because the process consumes CO_2, a global warming gas.[1] H_2O reforming of CH_4 gives syngas with a higher H_2/CO ratio than does CO_2 reforming, and these two processes can be used in combination to adjust the H_2/CO ratio.[7−10] For example, syngas with a H_2/CO ratio of 2 is used for gas-to-liquid (GTL) technology,[11−13] such as the production of ultraclean liquid fuels via the Fischer−Tropsch process.[11−18] To increase the efficiency of GTL processes, reforming should be performed at high pressure (>2 MPa) with low O/C and H/C ratios in the feed gas. However, the risk of catalyst degradation due to coking increases under such conditions.[7,19,20] Noble metal-based catalysts are less sensitive to carbon deposition, but are expensive.[7,8,21] Of the various supported metal catalysts,[22−24] Ni and Co supported on MgO, formed by reduction of the corresponding MgO solid solutions, are effective catalysts and are resistant to coking and sintering during CH_4 reforming with H_2O and CO_2.[11,19,25−27] The solid-solution preparation method has advantages over general impregnation methods because the former results in the formation of smaller metal particles that interact more strongly with the MgO support. However, after this catalyst is calcined at high temperature to increase its thermal stability, the amount of zerovalent metal

Received: November 15, 2012
Revised: May 22, 2013
Published: May 27, 2013

exposed to the feed gas is low, owing to the poor reducibility of Ni and Co. For example, only 2.9% of Ni atoms are reduced when reduction is carried out at 1123 K for 0.5 h.[28] The low amount of zerovalent metal exposed leads to oxidative deactivation of the catalysts at the low temperatures commonly found at the inlet of reformers under real-world operation conditions.[28,29] Adding small amounts of a noble metal retards Ni oxidation in the solid-solution catalysts,[28,30,31] and the resulting catalysts resist oxidative deactivation owing to increased Ni^{2+} and Co^{2+} reduction and enhanced dissociative adsorption of CH_4;[28] however, the use of even trace amounts of noble metals is not economical.

As an alternative means to increase the amount of exposed zerovalent metal in these catalysts, we previously explored the addition of inexpensive 11 mol % Cr to Co + Ni and found that the addition promotes Co^{2+} and Ni^{2+} reduction and retards oxidative deactivation of a $Co_{0.054}Ni_{0.018}Mg_{0.93}O$ solid-solution catalyst.[29] In that research, a Co and Ni bimetallic catalyst was used to control the kinetics of the reaction of CH_4, CO_2, and H_2O.[32,33] However, the CoNi alloy particles are large (>50 nm) and, thus, are subject to coking during long-term reactor operation.[34,35] Furthermore, we did not study the state or location of the Cr.

In this study, we investigated the influence of Cr load on the physicochemical properties of Cr−$Co_{0.054}Ni_{0.018}Mg_{0.93}O$ solid solutions using X-ray photoelectron spectroscopy (XPS), X-ray absorption near-edge structure (XANES) and extended X-ray absorption fine structure (EXAFS) measurements along with scanning transmission electron microscopy with energy-dispersive X-ray (STEM−EDX) analysis. The results elucidated the state and function of Cr during H_2 activation. On the basis of the results, we prepared a 0.11 mol % Cr−$Co_{0.054}Ni_{0.018}Mg_{0.93}O$ solid-solution catalyst with abundant small alloy particles on the catalyst particles. The catalyst resisted coking and oxidative deactivation in $CH_4/CO_2/H_2O$ reforming at high pressure (2.1 MPa), even under accelerated degradation conditions.

EXPERIMENTAL SECTION

Preparation of Catalysts. Co_3O_4−NiO/MgO (Co/Ni = 3/1 mol/mol, 10 wt % total) was prepared by wet impregnation of an aqueous solution of $Co(NO_3)_3{\cdot}6H_2O$ (Wako Pure Chemical Industries, Japan) and $Ni(NO_3)_2{\cdot}6H_2O$ (Wako) with MgO (JRC-MGO500A, Catalysis Society of Japan, Japan), which had been precalcined at 1073 K for 5 h. Chromium, in the form $Cr(NO_3)_3{\cdot}9H_2O$ solutions (Wako) [Cr/(Co + Ni) = 0.11−61 mol %, refereed to x mol % Cr], was added simultaneously with the Co and Ni precursors. The samples were dried at room temperature and at 343 K overnight and then calcined at 723 K for 5 h in flowing air. All the catalysts, referred to as x mol % Cr−$Co_{0.054}Ni_{0.018}Mg_{0.93}O$ solid-solution catalysts, were prepared by calcination at 1373 K for 5 h in static air. The resulting powders were pressed into pellets at 1.2 MPa for 3 min. The pellets were crushed and sieved to obtain grains with diameters between 250 and 500 μm. All the catalyst grains were activated ex situ with H_2 at 1173 K for 20 h.

Characterization of Catalysts. The specific surface areas of the catalysts were measured with a BELSORP-mini (BEL Japan, Japan) at 77 K with N_2 as the analysis gas. The amount of H_2 chemisorbed at 323 K (a measure of the amount of exposed zerovalent metal) and the amount of O_2 absorbed at 1123 K (a measure of the total reduction degrees of Co and Ni) were determined by pulse methods as follows. The activated catalysts were reduced in situ at 973 K for 1 h and cooled to 323 K under Ar. At 323 K, H_2 was pulsed over the catalysts. Subsequently, the catalysts were heated to 1123 K in an Ar flow, and O_2 was pulsed over them at 1123 K. H_2 and O_2 uptake amounts were measured with a thermal conductivity detector for these experiments. To calculate the amount of exposed zerovalent metal, we assumed that each metal site chemisorbed one hydrogen atom. The total reduction degrees of Co and Ni were calculated by assuming oxidation of Ni^0 and Co^0 to NiO and CoO.

X-ray diffraction analysis was performed with a RINT-2000 X-ray diffractometer (Rigaku, Japan) with monochromatized Cu Kα radiation. Crystallite sizes of MgO were calculated from line broadening with the Scherrer equation.[36]

X-ray photoelectron spectra were obtained with an ESCA-850 spectrophotometer (Shimadzu, Japan). The samples were transferred to the chamber of the XPS instrument before and after H_2 activation. To investigate the state of the Cr in the bulk as well as surface of the catalyst particles, Ar^+ ion beam etching of the samples was conducted at an energy of 2 keV and a current of 20 mA. The binding energy was calibrated, assuming that the Mg 2p core level was 51.5 eV .[37] Throughout the measurements, the Mg 2p peak did not split and retained the same shape.

X-ray absorption spectra were measured at the Photon Factory (Japan) on the BL9A and BL12C beamlines with a Si(111) monochromator. The spectra of the catalysts were measured before and after H_2 activation. The activated catalysts were again reduced in H_2 at 973 K for 1 h. After the catalysts were cooled to room temperature, their X-ray absorption spectra were measured without exposure to air. X-ray absorption spectra were recorded at the Cr K-edge (5988.8 eV) and analyzed with the Athena. The k^3-weighted EXAFS oscillation in the 2−10 $Å^{-1}$ region was Fourier transformed. In addition, the absorption spectra of $MgCrO_4$ in MgO, 1.1 mol % Cr/MgO, and $MgCr_2O_4$ were measured as references. For that purpose, 10 wt % Cr/MgO was prepared by wet impregnation of $Cr(NO_3)_3{\cdot}9H_2O$ solutions and dried at 343 K overnight before being calcined at 723 K for 5 h in flowing air. Powder X-ray diffraction was used to confirm that Cr existed as $MgCrO_4$ in the resultant 10 wt % Cr/MgO. In addition, a 1.1 mol % Cr/MgO sample was prepared by the impregnation method and further calcined in air at 1373 K for 5 h. $MgCr_2O_4$ was prepared by a polymerizable complex method (based on polyesterification between citric acid and ethylene glycol) from $Cr(NO_3)_3{\cdot}9H_2O$ and $Mg(NO_3)_2{\cdot}6H_2O$ and was calcined at 1173 K. Formation of $MgCr_2O_4$ was confirmed by X-ray diffraction analysis.

HAADF-STEM and EDX analysis were carried out with a JEM-2100F microscope (JEOL, Japan) at an accelerating voltage of 200 keV. The samples were thinned to <100 nm by mechanical polishing and then subjected to Ar-ion milling, after which cross sections were observed. A beam size of 1 nm was used for EDX spot analysis.

Deposited carbon was quantified by a temperature-programmed oxidation method. After the reforming reaction, the catalyst was heated to 1273 K at a rate of 10 K min^{-1} in an O_2/Ar mixture (1/19, 30 mL min^{-1}). CO_x gases derived from deposited carbon were passed through a methanator and then monitored with a flame ionization detector.

Tests of Catalyst Activity. A sample of each catalyst (100−400 mg) was loaded into a tubular Inconel reactor passivated with an aluminum diffusion coating. After reduction

dx.doi.org/10.1021/cs400199b | ACS Catal. 2013, 3, 1564−1572

in situ with H_2 at 973 K for 1 h, the catalyst was cooled to reaction temperature, and the pressure was increased from 0.1 to 2.1 MPa. Then a 1/1/0.5 (mol/mol) $CH_4/H_2O/CO_2$ mixture [1123 K, space velocity (SV) = 3000 h^{-1}], a 1/0.75/0.75 $CH_4/H_2O/CO_2$ mixture (873 K, SV = 3000 h^{-1}), or a 1/1.5 CH_4/H_2O mixture (923 K, SV = 72 000 h^{-1}) was passed over the catalyst. The reaction products were analyzed by gas chromatography with thermal conductivity detection (GC-8A, Shimadzu, Japan). After the reaction, the reactor was purged with Ar at the reaction temperature, and then the catalyst was cooled to room temperature and used for further analysis.

RESULTS AND DISCUSSION

Characterization of the Catalyst. The reduction degrees of Co and Ni after H_2 activation at 1173 K increased drastically from 8 to 50% with the addition of 0.11 mol % Cr, and a Cr load of ≥1.1 mol % resulted in almost complete reduction of Co^{2+} and Ni^{2+} in the solid solution (Figure 1A). In addition, a

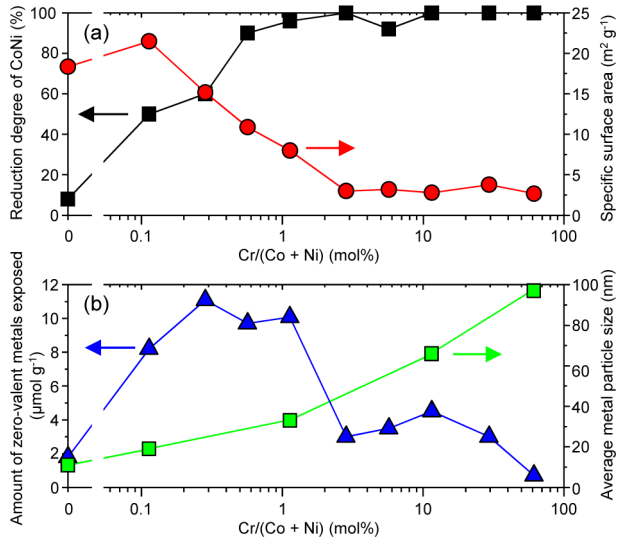

Figure 1. Influence of Cr load on physicochemical properties of the solid-solution catalysts after reduction at 1173 K for 20 h: (A) reduction degree of CoNi and specific surface area and (B) amount of zerovalent metal exposed and average metal particle size.

Cr load of 0.11 mol % increased the specific surface area of the catalysts from 17 to 20 m^2 g^{-1}. However, further increases in the Cr load induced sintering of the catalysts: the specific surface area of the catalysts decreased to 3 m^2 g^{-1} at Cr loads of ≥2.8 mol %. Such catalyst sintering was facilitated by an increase in the crystallite size of MgO (Supporting Information Figure S1). In short, addition of Cr promoted reduction of Co^{2+} and Ni^{2+} but induced sintering of the support material, leading to aggregation of metal particles (Figure 1B): the average metal particle size increases from 13 nm at 0 mol % Cr to 96 nm at 61 mol % Cr. These results provide a reasonable explanation for the observed changes in the amount of zerovalent metal exposed as a function of increasing Cr load (Figure 1B). The addition of 0.11 and 0.28 mol % Cr increased the amount of zerovalent metal exposed from 1.4 to 8.2 and 11 μmol g^{-1}, respectively, owing to a drastic increase in the reduction degree of Co and Ni. No such increases in reduction degree and amount of zerovalent metal exposed were reported previously when noble metals were added to improve the reducibility of Ni^{2+} or Co^{2+}.[28,30,31] In contrast, the amount of zerovalent metal exposed remained nearly the same when the Cr load was increased to 1.1 mol %, owing to the combined effect of increasing the reduction degree of Co and Ni and aggregation of the metal particles. Increasing the Cr load further to ≥2.8 mol % drastically decreased the amount of zerovalent metal exposed, owing to aggregation of the metal particles. Hence, we concluded that Cr acted as a glue for sticking the support materials to each other and thus induced aggregation of the metal particles in the presence of excess Cr at loads ≥0.28 mol %. To determine the mechanism by which Cr promoted Co^{2+} and Ni^{2+} reduction, we characterized the catalysts by means of XPS, XANES, EXAFS, and STEM−EDX analyses.

To determine the states of Cr, Cr $2p_{3/2}$ XP spectra of 11 mol % Cr−$Co_{0.054}Ni_{0.018}Mg_{0.93}O$ solid-solution catalysts before and after H_2 activation were measured (Figure 2). On the other

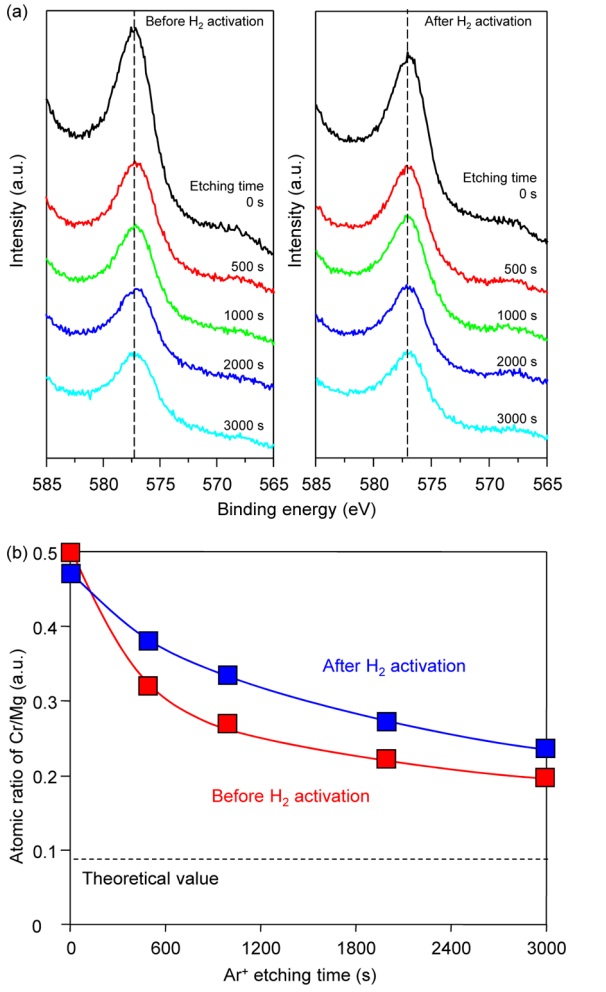

Figure 2. X-ray photoelectron spectra of Cr in 11 mol % Cr−$Co_{0.054}Ni_{0.018}Mg_{0.93}O$ solid-solution catalysts: (a) spectra of Cr $2p_{3/2}$ orbital before and after H_2 activation; (b) depth profile of the atomic ratio.

hand, XP spectroscopy was not sensitive enough for analysis of the 0.11 and 1.1 mol % Cr catalysts. Without Ar^+ etching, the peak positions of the samples before and after H_2 activation were 577.2 and 577.1 eV, respectively. Furthermore, Ar^+ etching and XPS measurements were repeated to investigate the state of the Cr in the bulk of the catalysts particles and atomic ratio of Cr/Mg. Irrelevance to the absence or presence

dx.doi.org/10.1021/cs400199b | ACS Catal. 2013, 3, 1564−1572

of the H_2 activation, the peak position was not shifted, even if Ar^+ etching was prolonged for 3000 s. On the other hand, peak positions of Cr_2O_3 and K_2CrO_4 were 576.9 and 579.7, respectively. These results indicate that Cr exists as a trivalent cation in the bulk as well as at the surface of the catalyst particles. Note that the Cr/Mg atomic ratio was decreased with increase in Ar^+ etching time and approached the value of the total concentration, 0.09, determined by ICP-AES measurements. Therefore, it was revealed that Cr^{3+} is abundant on the surface of the 11 mol % Cr−$Co_{0.054}Ni_{0.018}Mg_{0.93}O$ solid-solution catalyst before and after H_2 activation.

Although we carried out XRD measurements to investigate the structure of the phase including Cr, sensitivity of the methods was not sufficient for all the samples. To obtain information for the local structure of the Cr, we compared the Cr K-edge XANES spectra of 0.11−11 mol % Cr−$Co_{0.054}Ni_{0.018}Mg_{0.93}O$ solid-solution catalysts before and after H_2 activation with the spectra of Cr^0 foil, 1.1 mol % Cr/MgO calcined at 1373 K, $MgCr_2O_4$, and $MgCrO_4$ (Figure 3). We

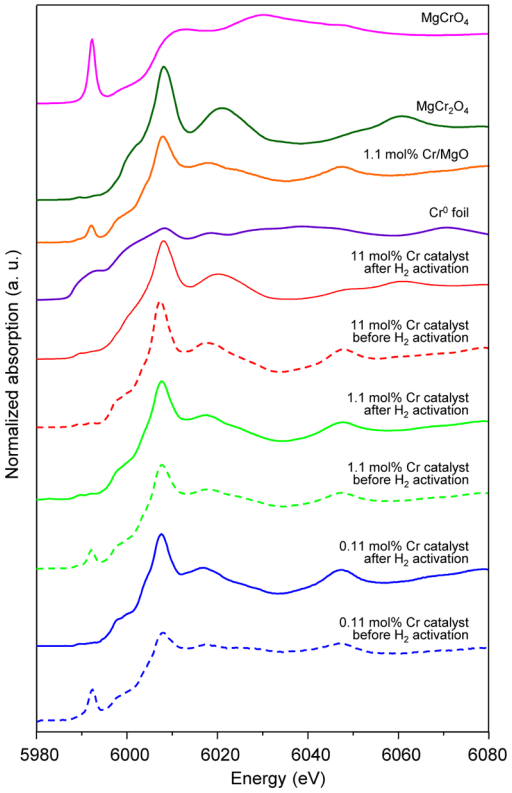

Figure 3. Cr K-edge XANES for Cr−$Co_{0.054}Ni_{0.018}Mg_{0.93}O$ solid-solution catalysts before and after H_2 activation at 1173 K.

chose these reference samples by consulting phase equilibrium diagrams for the MgO−Cr_2O_3[38] and Cr−Mg−O[39] systems. The phase equilibrium diagram[38] for the MgO−Cr_2O_3 system and the research reported by Thorp et al.[40] indicated formation of $Cr_xMgO_{1+1.5x}$ solid solution (<5 mol % Cr), where Cr^{3+} was isolated and substituted for Mg^{2+} in the MgO lattice, and $MgCr_2O_4$ (>5 mol % Cr) at 1373 K. Because peak positions of 1.1 mol % Cr/MgO calcined at 1373 K were different from those of $MgCr_2O_4$, we believe that the former sample contains mainly $Cr_xMgO_{1+1.5x}$ solid solution. On the other hand, at temperatures lower than 1173 K, formation of $MgCrO_4$ was predicted by the phase equilibrium diagram[39] for the Cr−Mg−O system.

The peak positions in the XANES spectra of the 0.11, 1.1, and 11 mol % Cr catalysts before H_2 activation were similar to the positions in the spectrum of the 1.1 mol % Cr/MgO, although the pre-edge peak decreased with an increase in the Cr load and disappeared for 11 mol % Cr catalyst. Here, it must be recalled that XPS measurements (Figure 2) revealed that Cr in 11 mol % Cr catalyst before H_2 activation was trivalent. Therefore, in combination with the results obtained by XANES and XPS, it was indicated that Cr^{3+} is included in the solid solution of 11 mol % Cr catalyst before H_2 activation. After H_2 activation at 1173 K, the 0.11 and 1.1 mol % Cr catalysts still exhibited spectra similar to the spectrum of the 1.1 mol % Cr/MgO except for the disappearance of the pre-edge band. Here, 0.11 and 1.1 mol % Cr catalysts before H_2 activation were prepared by calcination at 1373 K in static air after wet impregnation of Co, Ni, and Cr precursors. Although the phase equilibrium diagram for the MgO-Cr_2O_3[38] does not predict the formation of Cr^{6+} at 1373 K, these results indicate that some of the Cr^{3+}, probably on the surface of the catalyst, was oxidized to Cr^{6+}, formation of which was predicted by the phase equilibrium diagram[39] for the Cr−Mg−O system, during the cooling process after calcination. The Cr^{6+} was likely to be reduced to Cr^{3+} during H_2 activation.

In contrast, the spectrum of the 11 mol % Cr catalyst was similar to the spectrum of the 1 mol % Cr/MgO only before H_2 activation; after H_2 treatment, the spectrum was nearly identical to that of $MgCr_2O_4$. The valence of Cr in the compounds was in agreement with the results of XPS measurements.

We compared k^3-weighted Cr K-edge EXAFS oscillations and their Fourier transforms for the 1.1−11 mol % Cr−$Co_{0.054}Ni_{0.018}Mg_{0.93}O$ solid-solution catalysts with those for the reference samples (Figure 4). Although EXAFS spectroscopy was not sensitive enough for analysis of the 0.11 mol % Cr catalyst, we speculate that the state of Cr in this sample was similar to that in the 1.1 mol % Cr sample except for the $Cr^{6+}/(Cr^{6+} + Cr^{3+})$ ratio, owing to the similarity of the XANES spectra of the two catalysts. For the 1.1 mol % Cr catalyst before and after H_2 activation and the 11 mol % Cr catalyst before H_2 activation, the shape of the Cr K-edge EXAFS oscillations were similar to that of 1.1 mol % Cr/MgO. Furthermore, the first and second shell peaks in the FT of EXAFS spectra for these three samples and 1.1 mol % Cr/MgO were observed at the same position. These results support formation of solid solutions, as indicated by Cr K-edge XANES, where Cr^{3+} was isolated and substituted for Mg^{2+} in the MgO lattice. The excess single positive charge of Cr^{3+} with respect to Mg^{2+} was likely compensated for by the formation of a divalent cation vacancy for the 1.1 and 11 mol % Cr catalysts before H_2 activation. After H_2 activation at 1173 K, the 1.1 mol % Cr catalyst still existed as a solid solution.

On the other hand, for the 11 mol % Cr catalyst after H_2 activation, the shape of the Cr K-edge EXAFS oscillations was identical to that of $MgCr_2O_4$. The first and second shell peaks in the FT of EXAFS spectra for this sample were shifted to a slightly shorter position compared wtih the 11 mol % Cr catalyst before H_2 activation and identical to those of $MgCr_2O_4$. This means that a phase transition from a solid solution to a composite oxide with spinel phase, that is, $MgCr_2O_4$, occurred for the 11 mol % Cr catalyst during H_2 activation. Excess Cr^{3+} reportedly forms electrically neutral $MgCr_2O_4$ clusters that provide their own internal charge compensation.[40]

dx.doi.org/10.1021/cs400199b | ACS Catal. 2013, 3, 1564−1572

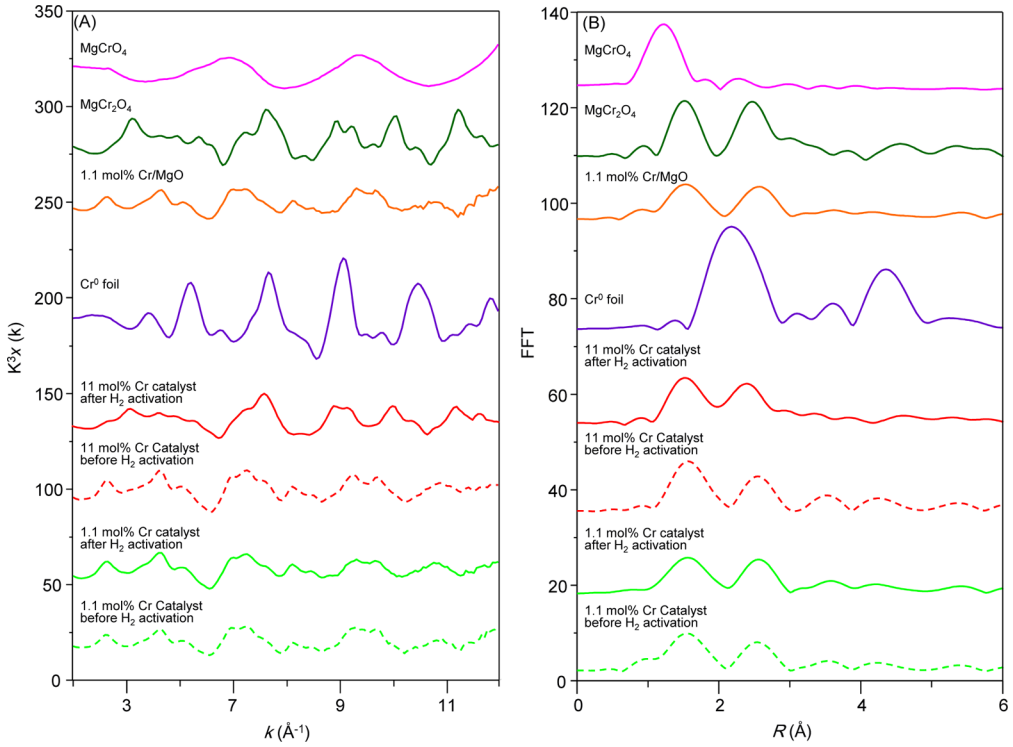

Figure 4. . k^3-Weighted Cr K-edge EXAFS oscillations (A) and their Fourier transforms (B) for Cr−$Co_{0.054}Ni_{0.018}Mg_{0.93}O$ solid-solution catalysts before and after H_2 treatment at 1173 K.

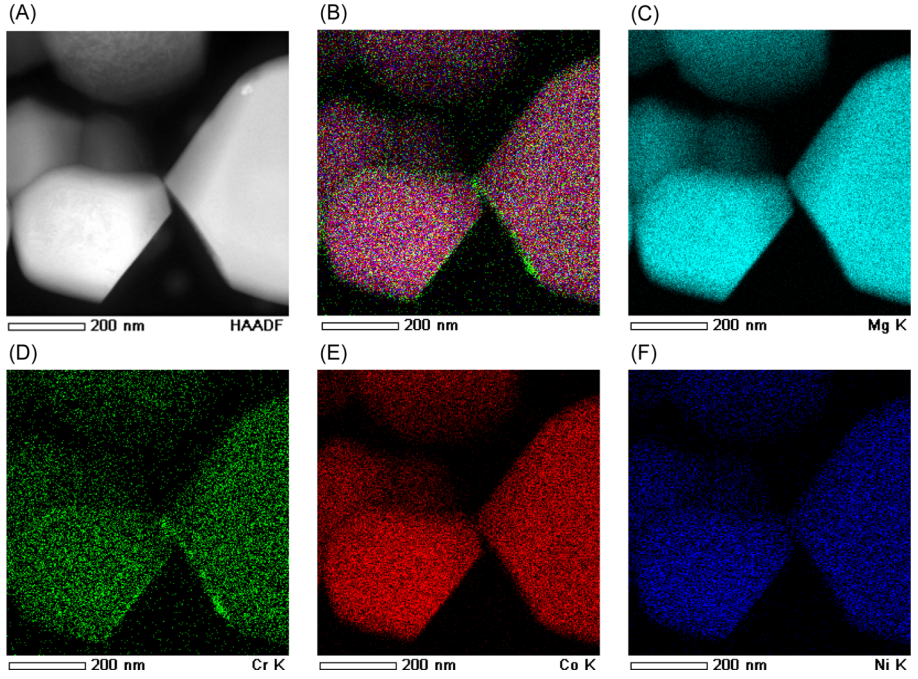

Figure 5. (A) HAADF−STEM image, (B) reconstructed overlay image of the maps shown in panels D−F, (C) Mg−K STEM−EDX map, (D) Cr−K STEM−EDX map, (E) Co−K STEM−EDX map, and (F) Ni−K STEM−EDX map for the 11 mol % Cr−$Co_{0.054}Ni_{0.018}Mg_{0.93}O$ solid-solution catalyst before H_2 activation.

We used high-angle annular dark field (HAADF) STEM and EDX elemental mapping to investigate the location of the Cr in the 0.11−11 mol % Cr−$Co_{0.054}Ni_{0.018}Mg_{0.93}O$ solid-solution catalysts before H_2 activation. The samples were thinned to <100 nm thickness by mechanical polishing and were then subjected to Ar ion milling, after which cross sections were observed. At this thickness, the surface and bulk of the catalyst particles, which had diameters of >200 nm, were discriminable in the STEM images. Mg, Co, and Ni were distributed homogeneously throughout the surface and bulk of the particles in the 11 mol % Cr catalyst (Figure 5), indicating that Co^{2+} and Ni^{2+} were dissolved into the bulk of the MgO particles and that a homogeneous solid solution was formed by calcination at 1373 K. These results conflict with our hypothesis that the

dx.doi.org/10.1021/cs400199b | ACS Catal. 2013, 3, 1564−1572

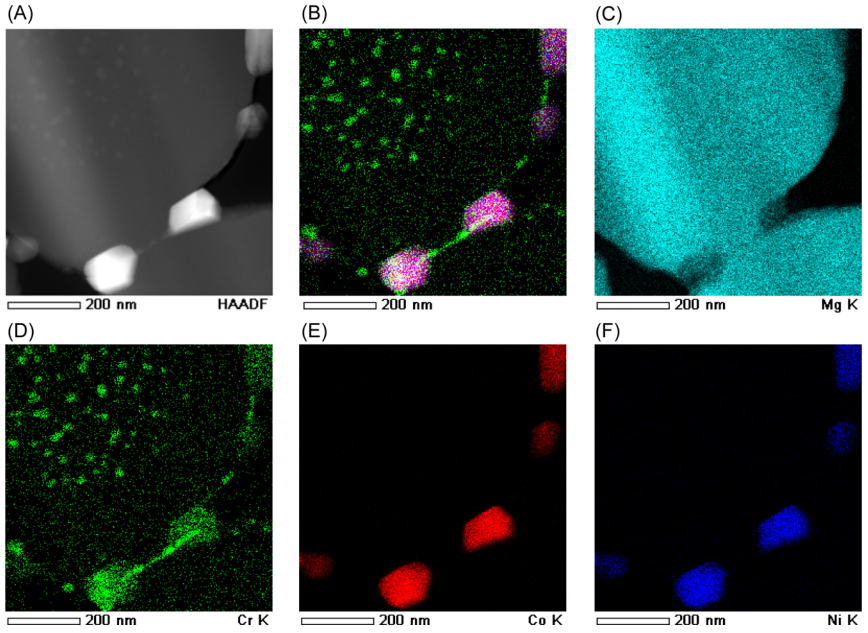

Figure 6. (A) HAADF−STEM image, (B) reconstructed overlay image of the maps shown in panels D−F, (C) Mg−K STEM−EDX map, (D) Cr−K STEM−EDX map, (E) Co−K STEM−EDX map, and (F) Ni−K STEM−EDX map for the 11 mol % Cr−$Co_{0.054}Ni_{0.018}Mg_{0.93}O$ solid-solution catalyst after H_2 activation.

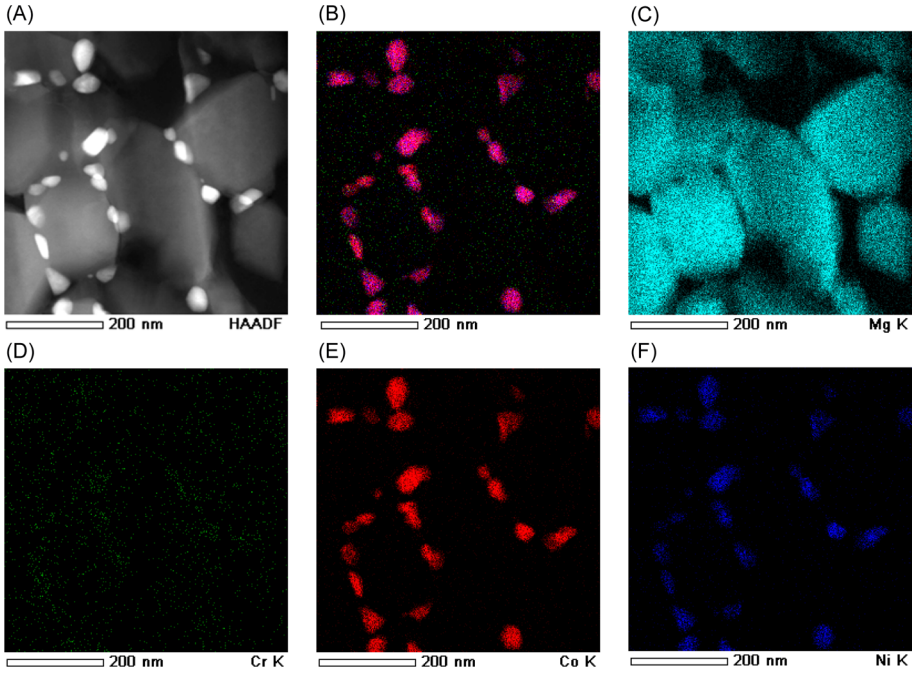

Figure 7. (A) HAADF−STEM image, (B) reconstructed overlay image of the maps shown in panels D−F, (C) Mg−K STEM−EDX map, (D) Cr−K STEM−EDX map, (E) Co−K STEM−EDX map, and (F) Ni−K STEM−EDX map for the 1.1 mol % Cr−$Co_{0.054}Ni_{0.018}Mg_{0.93}O$ solid-solution catalyst after H_2 activation.

addition of Cr promoted Co^{2+} and Ni^{2+} reduction by disturbing the dissolution of Co^{2+} and Ni^{2+} into MgO. In contrast, although Cr was present both on the surface and in the bulk of the catalyst particles, a reconstructed overlay image of Cr, Co, and Ni (Figure 5B) suggested that Cr was more abundant on the surface, which was in agreement with the results of XPS.

The homogeneous distribution of Co^{2+} and Ni^{2+} and the abundance of Cr on the surface of the 1.1 mol % Cr catalysts before H_2 activation are shown in Supporting Information Figures S2 and S3. EDX spot analysis indicated that Cr was abundant on the surface. For the 0.11 mol % Cr catalyst, a homogeneous distribution of Co^{2+} and Ni^{2+} is shown in Supporting Information Figure S4. Although even EDX spot analysis was not sensitive enough for analysis of Cr, we speculate that the location of the Cr in this sample was similar to that in the 1.1 and 11 mol % Cr samples. Cr must have existed as a trivalent cation in a $Cr_xCo_{0.054}Ni_{0.018}Mg_{0.93}O_{1+1.5x}$ solid solution, as indicated by the XPS, XANES, and EXAFS measurements. Furthermore, the excess single positive charge of Cr^{3+} with respect to Mg^{2+} was compensated for by the

dx.doi.org/10.1021/cs400199b | ACS Catal. 2013, 3, 1564−1572

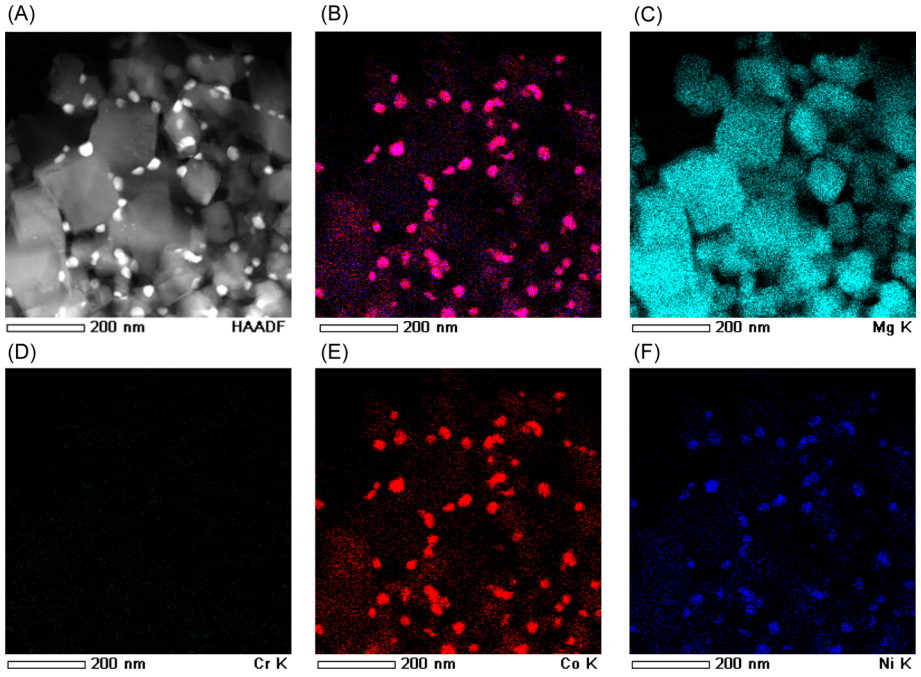

Figure 8. (A) HAADF–STEM image, (B) reconstructed overlay image of the maps shown in panels D–F, (C) Mg–K STEM–EDX map, (D) Cr–K STEM–EDX map, (E) Co–K STEM–EDX map, and (F) Ni–K STEM–EDX map for the 0.11 mol % Cr–$Co_{0.054}Ni_{0.018}Mg_{0.93}O$ solid-solution catalyst after H_2 activation.

formation of a divalent cation vacancy. Hence, diffusion of the Cr^{3+} from the surface to the bulk of the particles would not have readily occurred, and therefore, Cr^{3+} would have remained concentrated at the surface.

STEM and EDX elemental mappings of the 11 mol % Cr catalyst after H_2 activation (Figure 6) showed that Co and Ni were present only on the surface of the catalyst particles, indicating that upon activation, Co^{2+} and Ni^{2+} in the solid solution moved from the bulk to the MgO surface, where they were deposited as alloy particles. Because Cr was also visible at the same position as Co and Ni, we can say that Co, Ni, and trace amounts of Cr formed alloy particles. Furthermore, Cr was apparently much more abundant on the surface than in the bulk of the catalyst particles and was dispersed along the surface. Such an abundance of Cr on the surface was in agreement with the results of XPS. Chromium was also observed in the bulk of the catalyst particles as clusters with diameters of 10–20 nm. Considering these results in conjunction with the results of Cr K-edge XANES and EXAFS measurements, we can say that $MgCr_2O_4$ that formed during H_2 activation was distributed on the surface and in the bulk of the catalyst particles. In addition, $MgCr_2O_4$ existed at the catalyst particle boundaries, suggesting that Cr acted as a glue to adhere the catalyst particles to each other (Figure 6), thus inducing aggregation of the metal particles when the Cr load was ≥0.28 mol %. The 1.1 mol % Cr catalyst also showed CoNi particles only on the surface of the catalyst particles (Figure 7). Unlike the 11 and 1.1 mol % Cr catalysts, the 0.11 mol % Cr catalyst showed Ni and Co in the bulk as well as on the surface (Figure 8). This result was in agreement with the results revealing incomplete reduction of Co and Ni for this catalyst (Figure 1).

On the basis of the XPS, XANES, EXAFS, and STEM–EDX results for the 1.1 mol % Cr–$Co_{0.054}Ni_{0.018}Mg_{0.93}O$ solid-solution catalyst, we propose the following mechanism for the promotion of Co^{2+} and Ni^{2+} reduction in the catalyst by Cr (Scheme 1). Before H_2 activation (Scheme 1a), a $Cr_{0.00072}Co_{0.054}Ni_{0.018}Mg_{0.93}O$ solid solution existed. Because Cr^{3+} was dissolved in the solid solution of Mg^{2+}, Co^{2+}, and Ni^{2+},

Scheme 1. Mechanism of the Promotion of Co^{2+} and Ni^{2+} Reduction by Cr^{3+} in 1.1 mol % Cr–$Co_{0.054}Ni_{0.018}Mg_{0.93}O$: Catalyst Composition (a) before, (b) during, and (c) after H_2 Activation

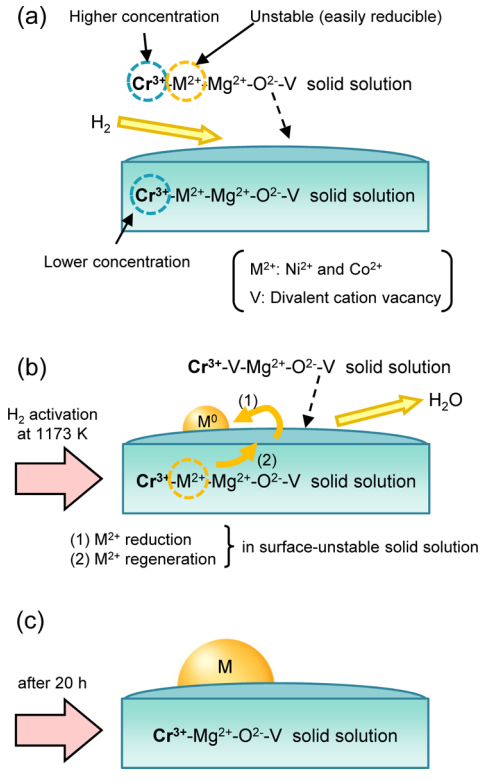

dx.doi.org/10.1021/cs400199b | ACS Catal. 2013, 3, 1564–1572

divalent cation vacancies formed to neutralize the charge of the solid solution. These phenomena destabilized Co^{2+} and Ni^{2+} (denoted M^{2+} hereafter) in the lattice of the MgO rock salt structure. Cr^{3+} was more abundant on the particle surface than in the bulk, indicating that M^{2+}, especially on the particle surface, was unstable, that is, easily reducible. At this stage, some of the Cr^{6+} also existed because some of the Cr^{3+} was oxidized during the cooling process after calcination at 1373 K. The Cr^{6+} is not depicted in Scheme 1 because Cr^{6+} was easily reduced in the subsequent reduction. When the catalyst was exposed to H_2 at 1173 K (Scheme 1b), M^{2+} in the surface-unstable solid solution was reduced to its metallic state, M^0, thus decreasing the surface concentration of M^{2+} and promoting M^{2+} diffusion from the bulk to the surface. The Cr^{3+} in the bulk also enhanced M^{2+} diffusion. M^{2+} reduction and regeneration were repeated until all the M^{2+} in the catalyst was reduced (Scheme 1c). Because Cr reduced M^{2+} more effectively at higher loads, M^{2+} reduction was insufficient at Cr load of 0.11 mol %, but aggregation of CoNi alloy was suppressed at the Cr load. In contrast, excess Cr loads apparently glued the catalyst particles together and induced sintering, which resulted in the aggregation of CoNi(Cr) alloy particles. It should be noted that the mechanism by which Cr promoted the reduction of M^{2+} is completely different from that of conventional noble metals: H_2 molecules dissociate to hydrogen species on the surface of noble metal particles, and the hydrogen species diffuse to the support surface and reduce M^{2+}.[28,30,31]

Behavior of the Catalysts. Because 0−11 mol % Cr−$Co_{0.054}Ni_{0.018}Mg_{0.93}O$ solid-solution catalysts showed stable activity under practical syngas generation conditions at a H_2/CO ratio of ~2 (2.1 MPa, $CH_4/H_2O/CO_2$ = 1/1/0.5, 1123 K, 20 h; Supporting Information Figure S5) and only minor coking (<0.1 wt %), we conducted tests under accelerated deterioration conditions to evaluate the influence of Cr load on catalyst activity. We plotted CH_4 conversion vs time on-stream at $CH_4/CO_2/H_2O$ = 1/0.75/0.75 (Figure 9A). Compared with the conditions used for real-world GTL processes, the reaction conditions studied here favored catalyst coking owing to the lower O/C and H/C ratios and lower temperature,[7] meaning that reactions conducted under these conditions serve as an accelerated coking test. For all the catalysts, we observed an induction period of 5−6 h, corresponding to the time required to replace the feed gas with the reactants in the cold trap (volume ~ 110 mL) at 2.1 MPa. After the induction period, CH_4 conversion reached approximately the equilibrium value. Although coke deposition was negligible for the 0 and 0.11 mol % Cr catalysts (<0.5 wt %), it increased with further increases in the Cr load (1.5 wt % for 1.1 mol % Cr and 12 wt % for 11 mol % Cr). Apparently, coking was more favored on catalysts with larger metal particles.[34,35] These results indicate that for the purposes of retarding coking, the Cr load should be ≤0.11 mol %, a value at which the average metal particle size was <20 nm.

We next plotted CH_4 conversion vs time on-stream at CH_4/H_2O = 1/1.5 at 873 K (Figure 9B). Compared wtih real-world GTL conditions, these conditions favored Co^0 and Ni^0 oxidation owing to the higher S/C and lower temperature,[28,29] meaning that reactions conducted under these conditions serve as an accelerated oxidative deactivation test. Again, a short induction period of 2 or 3 h was observed for all the catalysts. The 0 mol % catalyst was deactivated within 8 h, and the color turned from ash to beige during deactivation. These results

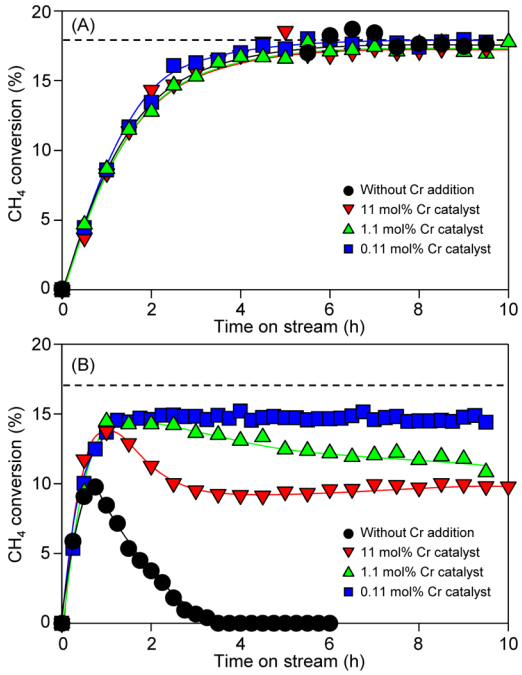

Figure 9. CH_4 conversion vs time on-stream under (A) accelerated coking conditions ($CH_4/CO_2/H_2O$ = 1/0.75/0.75, SV = 3000 h^{-1}, 923 K) and (B) accelerated oxidation conditions (CH_4/H_2O = 1/1.5, SV = 72 000 h^{-1}, 873 K). The dashed line shows equilibrium conversion.

indicate that the metals on the supports were oxidized by H_2O in the feed gas; that is, we ascribed the deactivation to Co^0 and Ni^0 oxidation. This conclusion is supported by an observed decrease in coking for all the catalysts (≤0.3 wt %). However, adding a trace amount of Cr (0.11 mol %) improved catalytic stability drastically, and the catalyst exhibited stable activity for 18 h. In contrast, increasing the Cr load to 11 mol % caused an initial reduction in activity (3−12 h for the 1.1 mol % Cr catalyst and 3−6 h for the 11 mol % Cr catalyst). We presume that Cr^0 on these catalysts was oxidized at the beginning of the reaction and that some portion of the Co^0 and Ni^0 was subsequently oxidized. These results thus indicate that the optimum Cr load was 0.11 mol %; at this load, the metal surface area was much higher than that at 0 mol % Cr, but Cr^0 was not present in excess in the alloy particles.

CONCLUSIONS

Our results indicate that a small amount of Cr^{3+} [Cr/(Co + Ni) = 0.11 mol %] in $Cr_xCo_{0.054}Ni_{0.018}Mg_{0.93}O_{1+1.5x}$ solid-solution catalysts efficiently catalyzed Co^{2+} and Ni^{2+} reduction and thus tailored the CH_4 reforming catalyst. Small alloy particles were well dispersed on the catalyst support, and thus, the metal surface area was high. The catalyst resisted coking and Co^0 and Ni^0 oxidation, even under accelerated deterioration conditions. However, these effects were limited to the relatively low Cr loads; excess Cr induced sintering of the catalyst particles, resulting in aggregation of alloy particles and thus in an increased risk of coking. Catalysts tailored by means of the new strategy described here, where composition of the surface layer on thermally stable catalyst support is adjustable, should be useful not only for reforming of other hydrocarbons but also for other types of high-temperature reactions.

dx.doi.org/10.1021/cs400199b | ACS Catal. 2013, 3, 1564−1572

■ ASSOCIATED CONTENT

Supporting Information

MgO crystallite size, STEM−EDX images, EDX spectra, and catalytic activities. These materials are available free of charge via the Internet at http://pubs.acs.org.

■ AUTHOR INFORMATION

Corresponding Author

*E-mail: nagaoka@oita-u.ac.jp.

Notes

The authors declare no competing financial interests.

■ ACKNOWLEDGMENTS

The authors thank M. Nomura, H. Abe, H. Nitani, Y. Niwa, and J. Nishino at Photon Factory, KEK, Japan for their support and guidance in the experiments. The authors thank Prof. K. Teramura for fruitful discussion of XAFS analysis.

■ REFERENCES

(1) Olah, G. A.; Prakash, G. K. S.; Goeppert, A. *J. Am. Chem. Soc.* **2011**, *133*, 12881−12898.
(2) Kerr, R. A. *Science* **2010**, *328*, 1624−1626.
(3) Howarth, R. W.; Ingraffea, A.; Engelder, T. *Nature* **2011**, *477*, 271−275.
(4) Jiang, M. *Environ. Res. Lett.* **2011**, *6*, 034014.
(5) Weber, C. L.; Clavin, C. *Environ. Sci. Technol.* **2012**, *46*, 5688−5695.
(6) Thomas, C, K. *Ecol. Econ.* **2011**, *70*, 1243−1249.
(7) Rostrup-Nielsen, J. R. In *Catalysis Science and Technology*; Anderson, J. R., Boudart, M., Eds.; Springer-Verlag: Berlin, Heidelberg, New York, Tokyo, 1984; Vol. *5*, Chapter 1.
(8) Rostrup-Nielsen, J. R. *Catal. Today* **1993**, *18*, 305−324.
(9) Lapszewicz, D. Q. *Catal. Today* **1994**, *21*, 551−560.
(10) Choudhary, V. R.; Rajput, A. M. *Ind. Eng. Chem. Res.* **1996**, *35*, 3934−3939.
(11) Ruckerstein, E.; Hu, Y. H. *Catal. Rev.* **2002**, *44*, 423−453.
(12) Choudhary, T. V.; Choudhary, V. R. *Angew. Chem., Int. Ed.* **2008**, *47*, 1828−1847.
(13) Kado, S.; Imagawa, K.; Kiryu, A.; Yagi, F.; Minami, T.; Kawai, H.; Kawazuishi, K.; Tomishige, K.; Nakamura, A.; Suehiro, Y. *Catal. Today* **2011**, *171*, 97−103.
(14) Dry, M. E. In *Catalysis Science and Technology*; Anderson, J. R.; Boudart, M., Eds.; Springer-Verlag: Berlin Heidelberg New York, 1981; Vol. *1*, Chapter 4.
(15) Khodakov, A. Y.; Chu, W.; Fongarland, P. *Chem. Rev.* **2007**, *107*, 1692−1744.
(16) Bezemer, G. L.; Remans, T. J.; van Bavel, A. P.; Dugulan, A. I. *J. Am. Chem. Soc.* **2010**, *132*, 8540−8541.
(17) Torres Galvis, H. M.; Bitter, J. H.; Khare, C. B.; Ruitenbeek, M.; Iulian Dugulan, A.; de Jong, K. P. *Science* **2012**, *335*, 835−838.
(18) Kang, J.; Cheng, K.; Zhang, L.; Zhang, Q.; Ding, J.; Hua, W.; Lou, Y.; Zhai, Q.; Wang, Y. *Angew. Chem., Int. Ed.* **2011**, *50*, 5200−5203.
(19) Tomishige, K.; Himeno, Y.; Matsuo, Y.; Yoshinaga, Y.; Fujimoto, K. *Ind. Eng. Chem. Res.* **2000**, *39*, 1891−1897.
(20) Nagaoka, K.; Takanabe, K.; Aika, K. *Chem. Commun.* **2002**, 1006−1007.
(21) Ashcroft, A. T.; Cheetham, A. K.; Green, M. L. H.; Vernon, P. D. F. *Nature* **1991**, *352*, 225−226.
(22) Venkataraman, K.; Wanat, E.; Schmidt, L. D. *AIChE J.* **2003**, *49*, 1277−1284.
(23) Wei, J.; Iglesia, E. *J. Catal.* **2004**, *224*, 370−383.
(24) Takehira, K.; Shishido, T.; Wang, P.; Kosaka, T.; Takaki, K. *J. Catal.* **2004**, *221*, 43−54.
(25) Yamazaki, O.; Nozaki, T.; Omata, K.; Fujimoto, K. *Chem. Lett.* **1992**, *21*, 1953−1954.
(26) Chen, Y.-g.; Tomishige, K.; Fujimoto, K. *Appl. Catal., A* **1997**, *161*, L11−L17.
(27) Ruckenstein, E.; Wang, H. Y. *Appl. Catal., A* **2000**, *204*, 257−263.
(28) Chen, Y.-g.; Tomishige, K.; Yokoyama, K.; Fujimoto, K. *Appl. Catal., A* **1997**, *165*, 335−347.
(29) Nagaoka, K.; Hashimoto, Y.; Sato, K.; Wakatsuki, T.; Nishiguchi, H.; Takita, Y. *Chem. Lett.* **2008**, *37*, 982−983.
(30) Li, D.; Nakagawa, Y.; Tomishige, K. *Appl. Catal., A* **2011**, *408*, 1−24.
(31) Nurunnabi, M.; Mukainakano, Y.; Kado, S.; Li, B.; Kunimori, K.; Suzuki, K.; Fujimoto, K.; Tomishige, K. *Appl. Catal., A* **2006**, *299*, 145−156.
(32) Nagaoka, K.; Takanabe, K.; Aika, K. *Appl. Catal., A* **2004**, *268*, 151−158.
(33) Takanabe, K.; Nagaoka, K.; Nariai, K.; Aika, K. *J. Catal.* **2005**, *232*, 268−275.
(34) Bitter, J. H.; Seshan, K.; Lercher, J. A. *J. Catal.* **1999**, *183*, 336−343.
(35) Tomishige, K.; Chen, Y.-g.; Fujimoto, K. *J. Catal.* **1999**, *181*, 91−103.
(36) Klug, H. P.; Alexander, L. E. *X-Ray Diffraction Procedures*; Wiley: New York, 1974.
(37) Wagner, D. C.; Riggs, M. W.; Davis, E. L.; Moulder, F. J; Muilenberg, E. G. *Handbook of X-ray Photoelectron Spectroscopy*; Perkin-Elmer: Eden Prairie, MN, 1978.
(38) Alper, M. A.; McNally, N. R.; Doman, C. R.; Keihn, G. F. *J. Am. Ceram. Soc.* **1964**, *47*, 30−33.
(39) Muller, O.; Roy, R.; White, B. W. *J. Am. Ceram. Soc.* **1968**, *51*, 693−699.
(40) Thorp, J. S.; Skinner, A. R.; Al-Hawery, A. S. *J. Magn. Magn. Mater.* **1989**, *82*, 277−286.